Effective one-dimensional approach to the source reconstruction problem of three-dimensional inverse optoacoustics

J. Stritzel, O. Melchert, M. Wollweber, and B. Roth
Hannover Centre for Optical Technologies, Nienburger Straße 17, 30167 Hannover, Germany
(Received 3 March 2017; revised manuscript received 15 August 2017; published 13 September 2017)

The *direct problem* of optoacoustic signal generation in biological media consists of solving an inhomogeneous three-dimensional (3D) wave equation for an initial acoustic stress profile. In contrast, the more defiant *inverse problem* requires the reconstruction of the initial stress profile from a proper set of observed signals. In this article, we consider an effectively 1D approach, based on the assumption of a Gaussian transverse irradiation source profile and plane acoustic waves, in which the effects of acoustic diffraction are described in terms of a linear integral equation. The respective inverse problem along the beam axis can be cast into a Volterra integral equation of the second kind for which we explore here efficient numerical schemes in order to reconstruct initial stress profiles from observed signals, constituting a methodical progress of computational aspects of optoacoustics. In this regard, we explore the validity as well as the limits of the inversion scheme via numerical experiments, with parameters geared toward actual optoacoustic problem instances. The considered inversion input consists of *synthetic* data, obtained in terms of the effectively 1D approach, and, more generally, a solution of the 3D optoacoustic wave equation. Finally, we also analyze the effect of noise and different detector-to-sample distances on the optoacoustic signal and the reconstructed pressure profiles.

DOI: 10.1103/PhysRevE.96.033308

I. INTRODUCTION

The *inverse* optoacoustic (OA) source reconstruction problem is concerned with the recovery of initial acoustic stress profiles from measured OA signals upon knowledge of the mathematical model that mediates the underlying diffraction transformation [1–3]. It is the conceptual analog of the *direct* OA problem (known as the OA *forward* problem), representing the calculation of a diffraction-transformed acoustic pressure signal at a given field point for a given initial acoustic stress profile on the basis of the OA wave equation [2–5]. In particular, once the source reconstruction problem is solved, one might use the obtained initial acoustic stress profile to solve a further *optical* inverse problem, i.e., the reconstruction of the optical absorption coefficient profile.

During the past few decades, the former problem has received much attention within the field of optoacoustics, due to its immediate relevance for medical applications (see, e.g., [6,7]) that are aimed at the reconstructions of "internal" OA material properties from "external" measurements. In this regard, current progress is mostly due to photoacoustic tomography (PAT) and imaging applications supporting different approaches [8–12]. In particular, note that the inversion input for PAT backpropagation approaches consists of a multitude of signals recorded on a surface enclosing the OA source volume.

In contrast to PAT, we introduce here an alternate OA approach that allows for the numerical reconstruction of initial stress profiles via inversion of signals from "single-shot" measurements. Therefore, we focus on the direct and inverse problem in the paraxial approximation to the full OA wave equation [4,13], where we allude to a numerical treatment of a linear one-dimensional integral equation, capturing the diffraction transformation of signals for an on-axis setting and allowing for an efficient solution of the direct and inverse OA problem. In particular, the effectively one-dimensional (1D) approach allows an approximate but highly efficient inversion of observed OA signals to initial stress profiles for the full 3D OA problem.

After developing and testing the numerical procedure, we assess how well the particular source reconstruction problem performs beyond the paraxial approximation by considering (i) signals obtained for the full OA wave equation in the acoustic far-field, and (ii) signals obtained using a detector with finite size. To the best of our knowledge, within the field of optoacoustics, no such numerical procedure has been discussed and put under scrutiny yet.

In Sec. II, we briefly summarize the theoretical background of OA signal generation and calculation. In Sec. III we elaborate on our numerical approaches, which yield forward and inverse solvers for the OA problem in the paraxial approximation, followed by a sequence of numerical experiments described in Sec. IV. We summarize and conclude upon our findings in Sec. VI.

II. THEORETICAL ASPECTS OF OA SIGNAL GENERATION

In the following subsections, we briefly review the theoretical foundation of the mechanism of OA signal generation. In this regard, in Sec. II A, we first detail a forward solution of the general problem based on the *OA Poisson integral*. After this, in Sec. II B, we allude to a particular "on-axis" variant of the forward problem based on the paraxial approximation, paving the way for a highly efficient inversion scheme in terms of a one-dimensional linear integral equation.

A. General OA signal generation—The OA Poisson integral

There are several microscopic mechanisms that may contribute to the generation of OA signals [14], but we restrict the subsequent theoretical discussion to the most dominant photothermal heating effect, i.e., thermal expansion. Further, we consider a pulsed OA working mode with a pulse duration

that is (i) significantly smaller than the thermal relaxation time of the surrounding material [15,16], realizing what is referred to as *thermal confinement*, and (ii) short enough to be represented by a δ function on the scale of typical acoustic propagation times [17], denoted by *stress confinement*.

Then, focusing on the acoustic aftermath of the thermoelastic expansion mechanism, the scalar excess pressure field $p(\vec{r},t)$ at time t and field point $\vec{r}$ can be related to an initial stress distribution $p_0(\vec{r})$ via the inhomogeneous OA wave equation [2,14]

$$\left[\partial_t^2 - c^2\vec{\nabla}^2\right]p(\vec{r},t) = \partial_t\, p_0(\vec{r})\,\delta(t), \tag{1}$$

wherein c signifies the speed of sound. Furthermore, the initial stress field is related to the volumetric energy density $W(\vec{r})$ [2,18], deposited in the irradiated region via absorption and photothermal heating by the short laser pulse, according to $p_0(\vec{r}) = \Gamma W(\vec{r})$. Therein, Γ refers to the Grüneisen parameter, an effective parameter describing the fraction of absorbed heat that is actually converted to mechanical stress. Note that in Eq. (1), temporal changes of the local photothermal heat absorption field $W(\vec{r})\delta(t)$ trigger stress waves that propagate through the medium and constitute the OA signal.

An analytic solution that yields the excess pressure $p(\vec{r},t)$ according to Eq. (1) is accessible through the corresponding Green's function in free space, establishing the OA Poisson integral [2,5,15]

$$p(\vec{r},t) = \frac{1}{4\pi c}\partial_t \int_V \frac{p_0(\hat{\vec{r}})}{|\vec{r}-\hat{\vec{r}}|}\delta(|\vec{r}-\hat{\vec{r}}| - ct)d\hat{\vec{r}}, \tag{2}$$

wherein V represents the "source volume" beyond which the initial stress $p_0(\vec{r}) = 0$ [19], and $\delta(\cdot)$ limiting the integration to a time-dependent surface centered at $\vec{r}$ and radially constraint by $|\vec{r}-\hat{\vec{r}}| = ct$.

B. Diffraction transformation in the paraxial approximation—The OA Volterra integral

In this article, we consider nonscattering compounds that consist of plane-parallel layers, stacked along the z direction of an associated coordinate system within the positive half-space. The acoustic properties within the bulk are assumed to be constant, whereas the optical properties are set to be constant within the layers but may differ from layer to layer, characterized by a depth-dependent absorption coefficient $\mu_a(\vec{r}) \equiv \mu_a(z)$; see Fig. 1. Then, for an inherently 2D plane-normal irradiation source profile $f(\vec{r}_\perp)$, the initial stress field can be factored according to

$$p_0(\vec{r}) = f(\vec{r}_\perp)\, g(z), \tag{3}$$

wherein $g(z)$ summarizes the effect of the absorptive properties of the layered medium in terms of a 1D axial absorption depth profile, which follows Beer-Lambert's law, i.e.,

$$g(z) = \mu_a(z)\exp\left\{-\int_0^z \mu_a(z')dz'\right\}, \tag{4}$$

for nonscattering media. Such a factorization of $p_0(\vec{r})$ is well justified. There are many examples in the literature in which experiments and their complementing simulations are in accord with the above constraints [18,20,21,23,24].

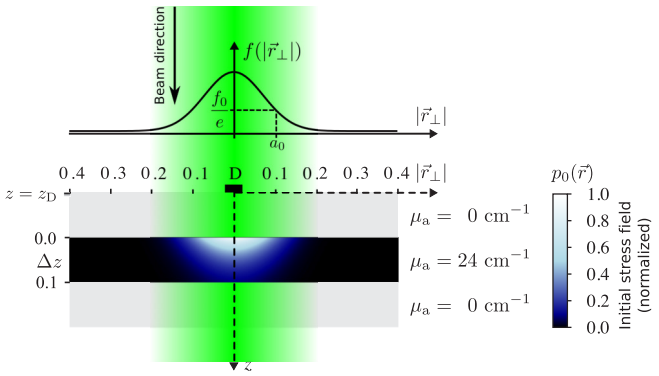

FIG. 1. Illustration of an OA setup with plane-normal irradiation source profile $f(|\vec{r}_\perp|)$ and a source volume consisting of possibly multiple stacked absorbing layers. The irradiation source exhibits a $1/e$-intensity radius of $|\vec{r}_\perp| = a_0$, and the different layers possess absorption coefficients μ_a as indicated in the figure. Here, the figure shows a single absorbing layer of width $\Delta z = 0.1$ cm. The initial stress field $\propto p_0(\vec{r})$ causes acoustic pressure waves that can be monitored as an OA signal at the detection point D, here located on the beam axis, i.e., at $|\vec{r}_\perp| = 0$, with distance $z_D < 0$ from the absorbing layer.

Further, let $f(\vec{r}_\perp)$ be an axially symmetric irradiation source profile with a Gaussian transverse profile, i.e.,

$$f(\vec{r}_\perp) = f_0\,\exp\left\{-|\vec{r}_\perp|^2/a_0^2\right\}, \tag{5}$$

wherein f_0 signifies the incident radiant exposure on the beam axis $|\vec{r}_\perp| = 0$, and a_0 defines the $1/e$ threshold of the beam intensity.

Under the above prerequisites, it can be shown that the diffraction transformation of laser-excited excess pressure profiles in the paraxial approximation of Eq. (1) at a detection point $\vec{r}_D$ along the beam axis, i.e., $p_D(\tau) \equiv p(\vec{r}_D,t)|_{(\vec{r}_\perp=0,\tau=t+z_D/c)}$, can properly be described in terms of a Volterra integral equation of the second kind [4,13],

$$p_D(\tau) = p_0(\tau) - \int_{-\infty}^{\tau} \mathcal{K}(t,\tau)\, p_0(t)\, dt, \tag{6}$$

here referred to as the *OA Volterra integral*. The change of argument in the description of the initial stress has to be understood as $p_0(\tau) = p_0(\vec{r})|_{(\vec{r}_\perp=0,\tau=t+z_D/c)}$. The Volterra operator, i.e., the second term in the equation above, describes the diffraction transformation experienced by the OA signal. It governs the propagation of acoustic stress waves in the OA on-axis setting with a Gaussian irradiation source profile via a convolution-type Volterra kernel $\mathcal{K}(t,\tau) = \mathcal{K}(\tau - t)$, wherein [13]

$$\mathcal{K}(\tau - t) = \omega_D\,\exp\{-\omega_D(\tau - t)\}. \tag{7}$$

Therein $\omega_D = 2c|z_D|/a_0^2$ denotes a characteristic OA frequency, related to the two "exterior" OA length scales given by (i) the distance $|z_D|$ between detection point and absorbing layer, and (ii) the transversal characteristic length scale a_0 of the irradiation source profile. The dependence of the diffraction transformation on the frequencies ω_D and $\omega_a = \mu_a c$, the latter signifying the characteristic frequency of the OA signal spectrum, is detailed in the literature; see, e.g.,

Ref. [13]. Note that in response to z_D and a_0, the frequency ω_D is either decreasing or increasing, defining the acoustic near-field (NF) and far-field (FF) from the value of the associated dimensionless diffraction parameter $D = \omega_D/\omega_a$ in the regimes $D < 1$ and $D > 1$, respectively.

Note also that the OA Volterra integral Eq. (6) not only allows us to solve the OA forward problem, i.e., the calculation of the excess pressure $p(z_D,\tau)$ given $p_0(\tau)$ and $\mathcal{K}(\tau,t)$, but it also makes it possible to solve the inverse OA source problem, i.e., the reconstruction of $p_0(\tau)$ given $p(z_D,\tau)$ and $\mathcal{K}(\tau,t)$, as will be detailed in the section below.

III. NUMERICAL IMPLEMENTATION OF THE OA FORWARD AND INVERSE SOLVERS

We will now elaborate on the numerical approaches we used in order to solve the OA forward and inverse problems; see Secs. III A and III B, respectively. Thereby, we also emphasize some important implications that the special case of a Gaussian transverse irradiation source profile has on our numerical implementation.

A. Forward solution

Regarding the solution process of the direct OA problem, i.e., the calculation of $p_D(\tau)$ for a given distribution of initial acoustic stress $p_0(\tau)$, we follow two distinct approaches. In Sec. III A 1, we first introduce a forward solver based on a numeric solution of the OA Poisson integral Eq. (2), followed by a more model-tailored solver based on a forward solution of the OA Volterra integral Eq. (6). For completeness, while the OA Volterra equation can be used for both the calculation of $p_D(\tau)$ as well as for the reconstruction of $p_0(\tau)$, we will subsequently need the Poisson integral based solver for benchmarking and generation of synthetic OA signals that serve as input for the inversion procedure. This is necessary in order to formally decouple the forward solution and inversion processes.

1. Forward solver based on the OA Poisson integral

Here, we opt for an implementation of Eq. (2) for layered media in cylindrical polar coordinates. The respective implementation is available as SONOS [25] and, although it is restricted to a solely z-dependent absorption coefficient, it allows for the efficient calculation of OA signals resulting from general irradiation source profiles with an axial symmetry at arbitrary detection points $\vec{r}_D = (\rho_D, z_D)$. Therein, z_D signifies the axial coordinate of the detection point in the reference frame in which the nearest absorbing layer has $z = 0$ (see Fig. 1), and ρ_D denotes the deviation of the detection point from the symmetry axis of the beam profile. Here, since we are only interested in the calculation of OA signals along the beam axis ($\rho_D = 0$), we can further simplify the numerical procedure detailed in Ref. [24] to some extent. That is, since the on-axis view of the irradiation source profile in the detection-point based reference frame is independent of the azimuthal angle, $f_D(\rho) = f_0 \exp\{-\rho^2/a_0^2\}$, the respective integration in a cylindrical polar representation of Eq. (2) can be carried out explicitly, resulting in the simplified expression

$$p_D(t) = \frac{\Gamma}{2c}\partial_t \int_\rho\int_z \rho \frac{f_D(\rho) g_D(z)}{\sqrt{\rho^2+z^2}} \delta(\sqrt{\rho^2+z^2} - ct)\, d\rho\, dz. \tag{8}$$

Note that in the above equation, the distance z is to be measured with respect to the detection point D, with the nearest absorbing layer located at $z = |z_D|$. Further, the δ distribution might be interpreted as an indicator function that bins the values of the integrand according to the propagation time of the respective stress waves. This already yields a quite efficient numerical scheme to compute the OA signal $p_D(t)$ at the detection point, since the pending integrations can, in a discretized setting where $\rho_i = i\Delta_\rho$, $i = 0,\ldots,N_\rho$, and $\Delta_\rho = \rho_{\max}/N_\rho$ as well as $z_i = |z_D| + i\Delta_z$, $i = 0,\ldots,N_z$, and $\Delta_z = (z_{\max} - |z_D|)/N_z$, be carried out with time complexity of order $O(N_\rho N_z)$. During our numerical experiments, since we are only interested in the general shape of the OA signal, we set the value of the constants in Eq. (8) to $\Gamma/c \equiv 2/f_0$. Finally, so as to mimic the finite thickness Δw of the transducer foil in an experimental setup [24], we grant the option to average $p_D(t)$ at the detection point over a time interval $\Delta t = \Delta w/c$.

2. Forward solver based on the OA Volterra integral

While there exist standard procedures for the numerical (forward) solution of Volterra integral equations of the second kind, e.g., based on an approximation of the diffraction term in Eq. (6) in terms of a trapezoidal rule [26] (or other quadrature rules [27], for that matter), we can simplify the approach for a general kernel $\mathcal{K}(\tau,t)$ by capitalizing on the special form of the OA stress wave propagator. Since the latter is of convolution type, Eq. (6) can be solved for $p_D(\tau)$ via memoization [28]. As it turns out, in a discretized setting where $t_i = i\Delta_t$, $i = 0,\ldots,N$, $\Delta_t = t_{\max}/N$, and thus $\tau_i = t_i + z_D/c$, abbreviating $\mathcal{K}(\tau_i - \tau_j)$ and $p_0(\tau_i)$ as $\mathcal{K}_{i,j}$ and $p_{0,i}$, respectively, we have $\mathcal{K}_{i,i} = \omega_D$ and $\mathcal{K}_{i+2,i} = \mathcal{K}_{i+1,i}\exp\{-\omega_D\Delta_t\}$, yielding a recurrence relation that approximates the diffraction term according to

$$\begin{aligned} I_i &= \int_{\tau_0}^{\tau_i} \mathcal{K}(\tau_i - t')p_0(t')\,dt' \\ &= \left[\mathcal{K}_{i,0}p_{0,0} + 2\sum_{j=1}^{i-1}\mathcal{K}_{i,j}p_{0,j} + \mathcal{K}_{i,i}p_{0,i}\right]\frac{\Delta_t}{2} \\ &= I_{i-1}e^{-\omega_D\Delta_t} + \frac{\omega_D\Delta_t}{2}[p_{0,i-1}e^{-\omega_D\Delta_t} + p_{0,i}]. \end{aligned} \tag{9}$$

In the above expression, the trapezoidal approximation becomes exact in the limit $N \to \infty$. Consequently, the OA signal $p_{D,i} \equiv p_D(\tau_i)$ can be obtained by simply marching in time, i.e., $p_{D,i} = p_{0,i} - I_i$ ($i = 1,\ldots,N$) starting off at $p_{D,0} = p_{0,0}$, $I_0 = 0$, and updating I_i via Eq. (9).

Note that adopting a standard discretized scheme for the calculation of $p_D(\tau)$, set up for a general kernel $\mathcal{K}(\tau,t)$ [26], would yield an algorithm that terminates in time $O(N^2)$ since the full integral has to be recomputed at each time step due to the "wandering" upper bound. This would not mean much of an improvement over the full wave equation solver discussed

in Sec. III A 1 as one has $N \approx N_z$. However, since the OA stress wave propagator is actually of convolution type and can be decomposed into a product of exponential factors at each time step, we yield here a highly efficient custom forward solver with time complexity $O(N)$.

B. Inverse solution

In terms of the recurrence relation approach that yields the diffraction term in Eq. (6) at time step i via memoization [see Eq. (9)], the actual inversion step is only slightly more involved than the forward solution. That is, the inverse solution in terms of the OA Volterra integral equation can be accomplished by updating the values of $p_{\mathrm{D},i}$ and I_i in a leap-frog manner according to

$$p_{0,i} = \alpha\left[p_{\mathrm{D},i} + \left(I_{i-1} + \frac{\omega_{\mathrm{D}}\Delta_t}{2}p_{0,i-1}\right)e^{-\omega_{\mathrm{D}}\Delta_t}\right],$$

$$I_i = I_{i-1}e^{-\omega_{\mathrm{D}}\Delta_t} + \frac{\omega_{\mathrm{D}}\Delta_t}{2}[p_{0,i-1}e^{-\omega_{\mathrm{D}}\Delta_t} + p_{0,i}], \quad (10)$$

starting off at $p_{0,0} = p_{\mathrm{D},0}$, $I_0 = 0$, and $\alpha = [1 - (\omega_{\mathrm{D}}\Delta_t)/2]^{-1}$. Thus, the numerical expense of the Volterra integral based inverse solver amounts to only $O(N)$.

Considering a far-field (FF) setup wherein the distance between the detection point D and the absorbing layers is large, i.e., $z_{\mathrm{D}} \to \infty$, and the width of the irradiation source profile is narrow enough to ensure a diffraction parameter $D \gg 1$ (also referred to as the Fraunhofer zone [29], a parameter region important for various approximate OA imaging methods [11,31]), the OA signal $p_{\mathrm{D,FF}}(\tau)$ is related to the initial OA stress profile $p_0(\tau)$ via [13,18]

$$p_{\mathrm{D,FF}}(\tau) = \frac{1}{\omega_{\mathrm{D}}}\frac{d}{d\tau}p_0(\tau). \quad (11)$$

Thus, in the FF approximation the initial stress profile $p_{0,\mathrm{FF}}(\tau)$ might be obtained by numerical quadrature using the above equation.

For completeness and so as to establish a broad computational foundation for the effectively 1D approach to inverse optoacoustics, note that the linear Volterra integral Eq. (6) might also be solved in terms of a Picard-Lindelöf iteration scheme [32], wherein a properly guessed approximate solution is improved successively until certain convergence criteria are met.

IV. NUMERICAL EXPERIMENTS

The simulation parameters used for the subsequent numerical experiments are geared toward actual "laboratory" parameters for existing polyvinyl alcohol hydrogel (PVA-H) -based tissue phantoms used in the combined experimental and numerical study reported in Ref. [24]. These consist of melanin-doped absorbing layers in between two layers of clear PVA-H, quite similar to the setup illustrated in Fig. 1. Here, we assume that the PVA-H layers are nonabsorbing and that the melanin-doped layer exhibits an absorption coefficient of $\mu_a = 24\ \mathrm{cm}^{-1}$. Although the irradiation source profile in such an experimental setting is usually assumed to be of "top-hat" type [18,21,24] (e.g., Ref. [24] report an overall $1/e$ radius of approximately 1.2 cm), we assume here an effective Gaussian beam profile with $1/e$ radius $a_0 = 0.1$ cm to suit the effectively 1D theoretical approach described in Sec. II B. This stimulating light beam meets the absorbing layer at $z = 0$ and leaves it at $z = \Delta z$. The resultant acoustic signal is computed for a field point located along the beam axis at position $z = z_{\mathrm{D}} < 0$.

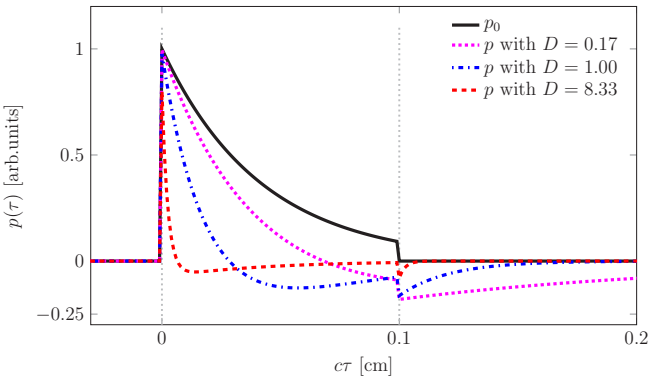

FIG. 2. Forward calculation of OA signals $p(\tau)$ in the framework of the Volterra integral equation. In this figure, p_0 (black solid lines) indicates the on-axis profile of the initial stress according to Eq. (4). The figure illustrates the change in shape of the OA signals as perceived at detection points with increasing detector-to-layer distance $z_{\mathrm{D}} = -0.02$ cm (magenta dotted line), -0.1 cm (blue dash-dotted line), and -1 cm (red dashed line), characterized by the diffraction parameters $D = 0.17$, 1.0, and, 8.33, respectively.

A. Forward and inverse solution within the OA Volterra framework

In the first series of numerical experiments, we deliberately stayed within the framework of the paraxial approximation [33], i.e., we accomplished the forward and inverse calculations by means of the solvers derived from the OA Volterra equation. Such an approach might be considered as committing an inverse crime [34], i.e., performing a (putative) trivial inversion of synthetic data obtained by first solving the forward problem in terms of the same exact model. However, here we use this approach as a proof of principle and consider an independent forward solver (with no connection to the Volterra-based solver) in subsequent sections. Although there is a wealth of literature discussing OA signals and their change in shape upon advancing from a measurement point located in the acoustic NF to a point in the FF (see, e.g., Refs. [4,13,29]), we first aimed at briefly illustrating the respective diffraction triggered signal changes for our particular single-layer setup by considering different values of z_{D}.

In this regard, Fig. 2 illustrates the forward calculation of OA signals in a discretized setting, where $z_i = z_{\min} + i\,\Delta_z$, $i = 1, \ldots, N$, and $\Delta_z = (z_{\max} - z_{\min})/N$, starting from an absorption profile obtained using Eqs. (3) and (4), i.e., following Beer-Lambert's law for pure absorbers. Here, we used $z_{\min} = 0.0$ cm, $z_{\max} = 0.1$ cm, $N = 300$, as well as $c = 1$, thus $\tau_i = z_i$. The general shape of the OA NF signal, characterized by the diffraction parameter $D = 0.17$, is still strongly reminiscent of the shape of the absorption profile. However, the initial compression phase has already noticeably transformed by diffraction, giving rise to an extended

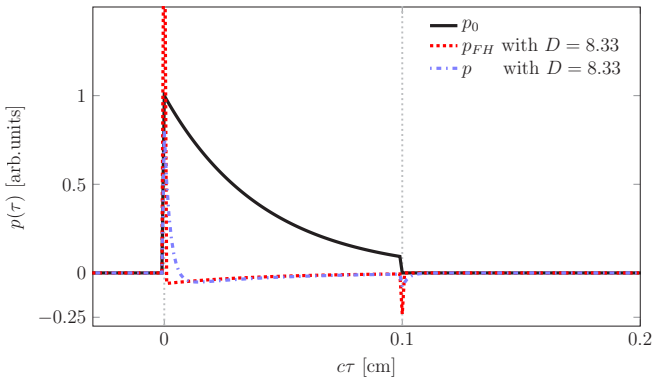

FIG. 3. Forward calculation of OA signals in a far-field approximation considering Eq. (11). In this figure, p_0 (black solid lines) indicates the on-axis profile of the initial acoustic stress. The figure illustrates the difference in the approximate FF formula, resulting in the signal p_{FH} (red dashed curve), relative to the exact solution p (red dash-dotted curve) at $z_{\mathrm{D}} = -1$ cm, i.e., $D = 8.33$.

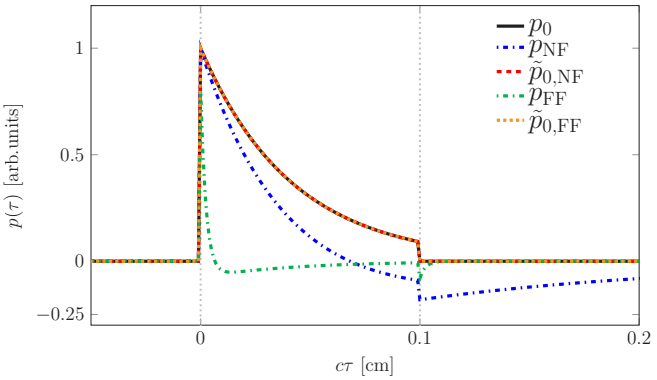

FIG. 4. Reconstruction of the initial acoustic stress $\tilde{p}_0$ from computed OA signals p upon knowledge of the diffraction propagator $\mathcal{K}$ in the acoustic NF ($\tilde{p}_{0,\mathrm{NF}}$) at $z_{\mathrm{D}} = -0.02$ cm, i.e., $D = 0.17$, and the acoustic FF ($\tilde{p}_{0,\mathrm{FF}}$) at $z_{\mathrm{D}} = -1.0$ cm, i.e., $D = 8.33$. The OA source reconstruction is accomplished with the leap-frog algorithm introduced in Sec. III B. In either case, the reconstructed stress profiles perfectly match the true initial stress profiles p_0.

rarefaction phase above a retarded signal depth of ≈0.08 cm, extending well beyond the signal depth that characterized the end of the absorbing layer. In contrast to this, the borderline NF ($D = 1.0$) and FF ($D = 8.33$) signals allow for a proper OA depth profiling: both feature a pronounced compression peak that signals an increase of the absorption coefficient μ_a at $z = 0$ cm, followed by an extended rarefaction phase until a sharp rarefaction dip signals a sudden decrease of the absorption coefficient at $z = 0.1$ cm continued by a further rarefaction phase rapidly decaying in amplitude. Since in the acoustic FF $p(\tau)$ is related to $p_0(\tau)$ via differentiation [see Eq. (11)], the peak value of the initial compression phase shifts toward the inclination point of the leading edge of $p_0(\tau)$ as D increases. As is evident from Fig. 3, the simplified calculation of the OA signal in the FF approximation according to Eq. (11) is already quite precise at $D = 8.33$, improving further in quality as $|z_{\mathrm{D}}| \to \infty$ (not shown). However, there is still a slight difference between the FF signal estimator $p_{\mathrm{FF}}(\tau)$ and the exact signal shape $p(\tau)$ for the genuine distribution of initial stress.

In a second set of numerical experiments, we aimed at solving the inverse OA problem, where the aim is to reconstruct the initial distribution of acoustic stress p_0 from the measured signal p upon knowledge of the OA stress propagator $\mathcal{K}$. As is evident from Fig. 4, the inverse solver based on the OA Volterra integral outlined in Sec. III B accomplishes this task in an efficient fashion: irrespective of whether the inversion is performed in the acoustic NF or FF (see Fig. 4), the reconstructed stress profiles $\tilde{p}_0$ perfectly match the exact initial stress profiles p_0.

B. Poisson-based forward and Volterra inverse solution

While the above computation and inversion of OA signals were performed using solvers, both derived within the framework of the OA Volterra integral equation, we subsequently consider the independent forward solver SONOS [25], detailed in Sec. III A 1, to yield synthetic input data for the source reconstruction process. Since the paraxial approximation on which the OA Volterra integral equation is based describes the underlying wave equation best at sufficiently large distances $|z_{\mathrm{D}}|$, we focus here on the inversion of signals in the acoustic FF only. This is shown in Fig. 5, where an OA signal, computed using the wave equation based forward solver, is inverted by means of the Volterra integral based inverse solver at $z_{\mathrm{D}} = -1.0$ cm (i.e., at $D = 8.33$). Note that while the initial distribution of acoustic stress features sharp edges at the boundary of the absorbing layer, the inverse estimate of the initial stress is more gently inclined. This is due to the temporal average over a time interval $\Delta t = 0.005$ cm$/c$, which is used to mimic the finite extension of a detector in an experimental setting (see the discussion in Sec. III A 1 and Ref. [24]).

To assess the improvement as well as the limits of the paraxial approximation upon increasing $|z_{\mathrm{D}}|$, we simulated

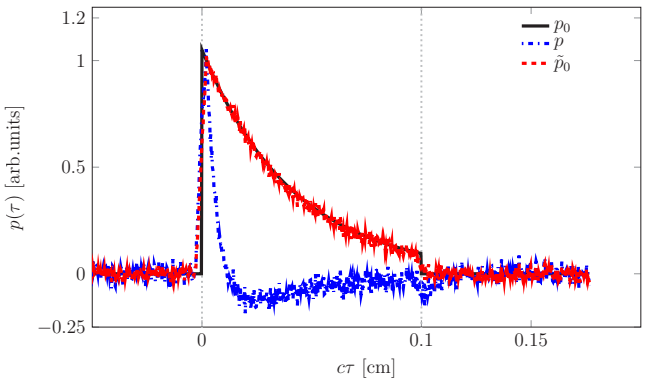

FIG. 5. Solution of the source reconstruction problem using the Volterra integral equation based inverse solver. The figure illustrates the reconstruction of the initial acoustic stress profile $\tilde{p}_0$ (dashed red line) from a FF signal p (dash-dotted blue line), calculated at $z_{\mathrm{D}} = -1$ cm. The true initial stress profile is given by p_0 (solid black line). Reconstruction starting from a genuine OA signal p that was superimposed by Gaussian white noise with a signal-to-noise ratio of 5.

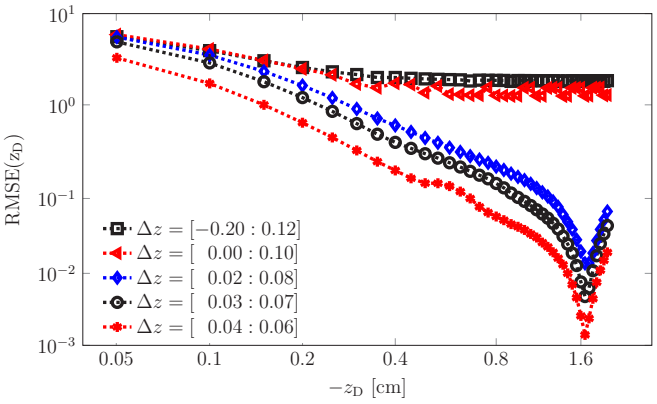

FIG. 6. Root-mean-square error (RMSE) between the true initial stress profile p_0 and the inverse estimate $\tilde{p}_0$ for increasingly narrow intervals $\Delta z \equiv [c\tau_- : c\tau_+]$ along the z and τ axes, respectively. Note that in a preprocessing step, p_0 was normalized and $\tilde{p}_0$ amplitude-adjusted, as detailed in the text.

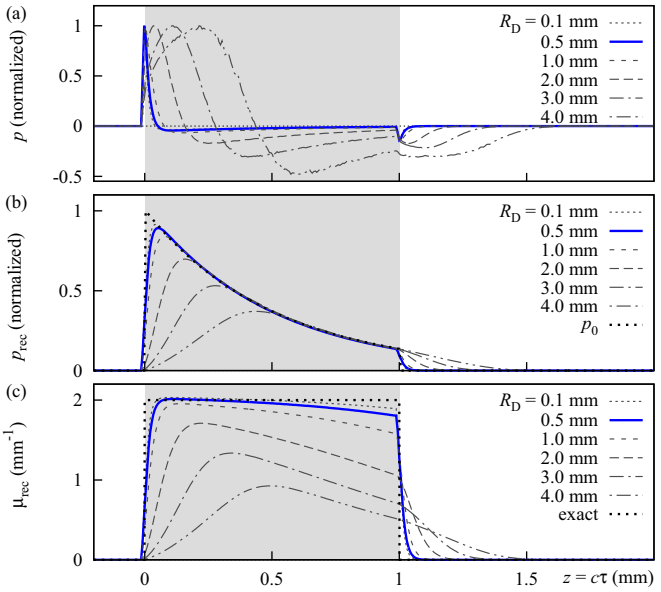

FIG. 7. Effect of a finite detector size on the OA signals and the reconstructed initial stress profiles. For the simulations, we considered detectors with a circular surface and different radii in the range $R_D = 0.1{-}4$ mm (for further details, see Sec. IV C). (a) OA signals obtained by solving the Poisson-like integral Eq. (2) and integration over the detector surface. (b) Reconstructed initial stress profiles obtained by inversion via Eq. (10). Note the exact initial stress profile indicated by the black dashed line. (c) Reconstructed absorption coefficient profile $\mu_{rec}(z)$. The exact absorption coefficient profile used to obtain the curves in (a) is indicated by the black dashed line. In either subfigure, the blue solid line emphasizes the curves for a detector radius $R_D = 0.5$ mm.

OA signals at various points in the range $z_D = -0.05, \ldots, -2.0$ cm. As pointed out in Sec. III A 1, the Poisson integral based forward solver yields an OA signal up to an amplitude factor. Hence, in order to be able to quantitatively compare the Volterra-based reconstruction $\tilde{p}_0$ to the true underlying p_0, we need to adjust the respective signal amplitudes. Therefore, in a preprocessing step we first normalized the initial stress profile so that $\int p_0(\tau)d\tau \equiv 1$, and subsequently we adjusted the amplitude of $\tilde{p}_0(\tau)$ so that the residual sum of squares $\mathrm{RRS}(\Delta\tau) = \sum_i^{M(\Delta\tau)}[p_0(\tau_i) - \tilde{p}_0(\tau_i)]^2$ is minimized within the tuning interval $\Delta\tau = [\tau_- : \tau_+]$ containing $M(\Delta\tau)$ sampling points. The resulting root-mean-square error $\mathrm{RMSE}(\Delta\tau) = \sqrt{\mathrm{RSS}(\Delta\tau)/M(\Delta\tau)}$ as a function of the detector-to-layer distance $|z_D|$ is shown in Fig. 6. As is evident from the figure, if the tuning interval encloses the region around the signal edges where the reconstructed stress profile is gently inclined (see the curve corresponding to $\Delta z \equiv c\Delta\tau = [-0.02 : 0.12]$ in Fig. 6), the RMSE above $-z_D \approx 0.2$ cm saturates at a finite value characterizing the signal mismatch around the edges. In contrast, if the tuning interval is chosen to be more narrow and to exclude those edge mismatches, e.g., in the range $\Delta z = [0.02 : 0.08]$, the RMSE decreases as $\propto |z_D|^{-3/2}$ until a limiting point at $z_D \approx -1.5$ cm is reached. This limiting point is solely due to the mesh width used to discretize the z axis. Here, we considered a mesh width of $dz = 2.5$ μm. Note that a smaller width dz would in turn allow to shift the limiting point to larger values of $|z_D|$ and to obtain highly precise reconstructed stress profiles also in the deep FF.

C. Effect of a finite detector size

Above, the forward calculation and inversion of OA signals were carried out for pointlike detectors. While this is acceptable in order to illustrate the principal algorithmic procedure, real "laboratory" experiments imply measurements via detectors of finite spatial extent. To assess the effect a finite-size detector has on both the obtained OA signals and the reconstructed initial stress profiles, we now consider a hypothetical setup involving a detector with a circular shape. In detail, the source volume was set up to contain an absorbing layer (in the xy plane) with $\mu_a = 2$ mm^{-1} extending from $z = 0$ to 1 mm. The irradiation source assumed a Gaussian beam profile with $1/e$ radius $a_0 = 0.5$ mm and plane-normal incidence. The circular detector with radius R_0 and a center along the beam axis was located at $z_D = -2.0$ cm in backward mode. The results of our numerical simulations for several detector radii in the range $R_0 = 0.1{-}4$ mm are summarized in Fig. 7. Therein, the particular value $R_D = 0.5$ mm, specifying the diameter of the transducer used in Ref. [24], is highlighted using a solid blue line. Technically, we realized the finite detector size by numerical integration of the excess pressure signal obtained by solving the Poisson-like integral Eq. (2) over the area of the detector using $N_R = 20$ radial samples. As is evident from Fig. 7(a), considering the above parameters a_0 and z_D, the local averaging enforced by a finite radius R_D has a discernible impact on the signal shape. While the curves for $R_D \leqslant 1$ mm still resemble the signal expected for a pointlike detector, the signal features for $R_D > 1$ mm are distinctly warped. A reconstruction of the initial stress profiles using the inversion formula Eq. (10) yields the curves p_{rec} shown in Fig. 7(b). Therein, the reconstructed initial stress profiles agree with the exact initial stress profile p_0 in the approximate range $z \in [R_D, 1\,\mathrm{mm}]$. In particular, for a realistic detector with

$R_D = 0.5$ mm, the reconstructed profile still agrees quite well with the exact initial profile.

D. Reconstruction of the optical absorption coefficient profile

As pointed out earlier, one particular use of the inversion procedure is that it allows us to reconstruct an approximate initial stress profile $p_{rec} \approx p_0$ that might in turn be used to estimate the optical absorption coefficient depth profile $\mu_{rec}(z)$ from the measured data p. That is, once p_{rec} is obtained, $\mu_{rec}(z)$ can be calculated via [22,23]

$$\mu_{rec}(z) = \frac{p_{rec}(z)}{\left[f_0 - \int_0^z p_{rec}(z')dz'\right]}; \tag{12}$$

see Fig. 7(c). Again, note that for $R_D < 1$ mm, the agreement of $\mu_{rec}(z)$ and $\mu_a(z)$ is still impressive. Further, assuming $\mu_a = \text{const}$ and performing simple fits to the form $f(z) \propto \exp(-\mu_a z)$ in the range $z \in [R_D, 1\text{ mm}]$ improves the results to $\mu_a = 2.055(3)\ \text{mm}^{-1}$ at $R_D = 0.5$ mm and $\mu_a = 2.02(1)\ \text{mm}^{-1}$ at $R_D = 4$ mm.

V. DISCUSSION

In addition to being an interesting inverse problem on its own, the optoacoustic source reconstruction problem allows us to tackle a further, solely optical inversion problem, namely the reconstruction of the optical absorption coefficient profile from the observed data. This is most useful when OA signals are recorded in the acoustic far-field and when the underlying optical absorption problem features unscattered absorption only. Note that such a scenario is considered in many experimental optoacoustic studies; see, e.g., Refs. [18,21,23,24]. Then, a protocol to retrieve the optical absorption coefficient profile from the measured OA signal reads as follows: given an OA signal recorded in the acoustic far-field, (i) solve the source reconstruction problem using the method proposed in Sec. III B, and (ii) recover the optical absorption profile from the initial acoustic stress, e.g., as illustrated in Sec. IV D. Note that the source reconstruction step is quite fast. The inversion of p to p_{rec} only needs about 0.3 s for the problem setup considered in Sec. IV C [profiled on a 2011 MacBook Air featuring a 1.7 GHz Intel Core i5 processor and 4 GB DDR3 running OS X Yosemite (Version: 10.10.3)]. Also, if the OA signals are recorded in the (diffraction-free) acoustic near-field, the source-reconstruction step is unnecessary and the optical parameters might be recovered directly [23].

Note that the description of the diffraction transformation of optoacoustic signals in terms of a linear integral equation in Sec. II B is not unique. A quite similar one-dimensional theoretical approach, built upon the assumption of plane acoustic wave propagation, yields the convolution integral [29,30]

$$p_r(\tau) = \omega_a \int_{-\infty}^{\infty} \mathcal{K}(\tau - \tau')\, p_0(\tau')\, d\tau', \tag{13}$$

by means of which the diffraction warped excess pressure profile $p_r(\tau)$ for a rigid (i.e., motionless) boundary can be related to the unperturbed stress profile $p_0(\tau)$. In the above equation, ω_a signifies a characteristic frequency of the OA signal spectrum. To facilitate a comparison with the proposed method, the excess pressure profile $p(\tau)$ for a free (i.e., pressure-release) boundary can be obtained from $p_r(\tau)$ by differentiation, $p(\tau) = \omega_a^{-1} \frac{d}{d\tau} p_r(\tau)$. Therein, the integral kernel $\mathcal{K}$ is equivalent to Eq. (7), and p can be obtained from p_0 even without knowing ω_a. The reconstruction of the initial stress profile from the above equation requires the inverse solution of an inhomogeneous Fredholm integral equation of the first kind, and it can be accomplished by deconvolution of the rigid-boundary excess pressure profile with the known integral kernel. To facilitate a comparison of both approaches, we consider the same simulation setup as in Sec. IV C (only for a pointlike detector) and perform the inversion using both methods. As is evident from Fig. 8, both reconstructed initial stress profiles are in good agreement with the exact profile. In either case, the integrated squared error $\int [p_0(\tau) - p_{rec}(\tau)]^2 d\tau \approx 0.0003$. Technically, we realized the inverse solution of Eq. (13) via Wiener deconvolution using a signal-to-noise ratio of infinity (since the synthetic data used for comparison were free of noise). Since the deconvolution is performed in the Fourier domain, back and forth transformation of the signal requires $O[N \log(N)]$ operations (as in Sec. III A 2, N refers to the number of samples comprising the signal). Hence, a conventional deconvolution approach requires a larger number of elementary operations, although it yields results with similar accuracy.

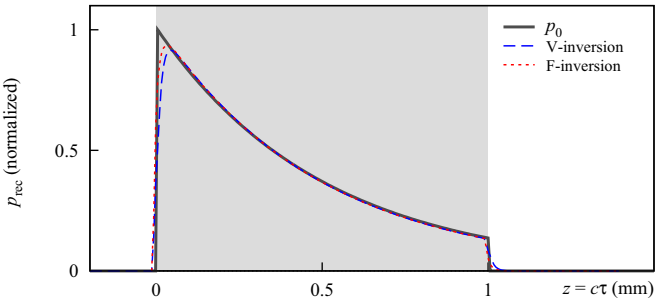

FIG. 8. Comparison of two inversion procedures derived from two different linear integral equations describing the diffraction transformation of OA signals. The (fast) numerical procedure based on the inverse solution of a Volterra integral equation of the second kind is indicated by the blue dashed line (labeled V-inversion), and the procedure based on the solution of an inhomogeneous Fredholm equation of the first kind (here accomplished using Wiener deconvolution) is indicated by the red dotted line (labeled F-inversion); for further details see Sec. V.

Regarding the applicability of the proposed algorithmic procedure, note that for the inversion of data obtained from the forward solution of the full 3D wave equation, the use of the paraxial approximation implies a set of restrictions that limit the inherent complexity of *feasible* problem setups. Since the set of feasible problem setups is only a subset of all possible problem setups, a pending question reads as follows: Under which circumstances can the proposed method be used to reconstruct the optical properties of *realistic* absorbing structures? To summarize, feasible problem setups need to comply with the following restrictions: (R1) the irradiation source profile is assumed to exhibit a Gaussian transverse profile, (R2) the optical properties of the sample are assumed to be invariant with respect to translation in the

plane perpendicular to the beam axis, and (R3) the field point at which the pressure transient is recorded is assumed to be located in the acoustic far-field. One might as well interpret these restrictions as a set of requirements. If one attempts the inversion of data (obtained from a realistic problem setup) with the proposed method, it needs to be clarified at first whether the problem at hand satisfies the above three requirements. In this regard, note that the proposed method implies adjustable parameters. That is, independent of the sample, the radius of the beam profile [related to (R1)] and the distance and spatial extension of the detector [related to (R3)] are variable within limits set by the optoacoustic measurement device.

Consider, e.g., the case of depth profiling for melanoma in a clinical application. If the sample is illuminated using a laser beam with a given diameter, the deposited (optical) energy might be viewed as taking an effective average value over the cross section of the beam. The smaller the beam diameter, the more *local* the beam-induced averaging of the samples optical properties. Now, if the detector is placed in the acoustic far-field (using buffer materials and proper impedance matching layers) and possesses a sufficient spatial and temporal resolution (which both affect the shape of the detected acoustic transient), the obtained data might be consistent with the restrictions imposed by the paraxial approximation. Further numerical studies that elaborate on the technicalities of the above issue are currently underway.

VI. SUMMARY AND CONCLUSIONS

In the presented article, we discussed OA signal generation in the paraxial approximation to the full 3D wave equation. This approach yields an effectively 1D linear integral equation that accounts for the diffraction transformation of propagating stress waves. We detailed numerical schemes to simulate OA signals in the forward direction, where we considered a 3D Poisson integral based solver as well as a highly efficient numerical scheme for the simplified 1D integral equation, derived on the basis of a standard quadrature rule and relying on the particular form of the OA integral operator. Therein, the algorithm for the full 3D wave equation terminates in time $O(N_\rho N_z)$, where N_ρ and N_z refer to the number of mesh points in the ρ and z directions, respectively. The algorithm facilitating a forward solution in the paraxial approximation terminates in time $O(N)$, wherein $N \approx N_z$ (see the discussion in Sec. III A). Thus, in a parameter range where the paraxial approximation is a valid approximation to the full 3D wave equation, the latter algorithm is much faster and a viable alternative to solving the full 3D Poisson integral. Further, regarding the inverse problem, we considered an efficient solver based on the 1D Volterra integral equation, allowing us to reconstruct initial stress profiles from "measured" signals. Therein, the inverse solver exhibits the same time complexity as the corresponding forward solver.

By means of numerical experiments, geared toward actual laboratory experiments for existing polyvinyl alcohol hydrogel (PVA-H) -based tissue phantoms reported in Ref. [24], we characterized OA signals in the acoustic near- and far-field. As supported by our simulations, considering the direct OA problem in the far-field, the 1D approach approximates the full 3D approach best. Regarding the inverse OA problem, we assessed the quantitative agreement between the reconstructed and true initial stress profiles as one proceeds toward the far-field.

Finally, from a point of view of computational theoretical physics, we explored an efficient numerical approach to the solution of the OA source reconstruction problem in terms of an effectively 1D linear integral equation. Although there exist several general numerical schemes for the forward and inverse solution of the underlying formulas, this particular inverse problem derived in the paraxial approximation of the OA wave equation has not yet received much attention in the literature [35].

ACKNOWLEDGMENTS

J.S. acknowledges support from the German Federal Ministry of Education and Research (BMBF) in the framework of the project MeDiOO (Grant No. FKZ 03V0826). O.M. acknowledges support from the Volkswagenstiftung within the "Niedersächsisches Vorab" program in the framework of the project "Hybrid Numerical Optics–HYMNOS" (Grant No. ZN 3061).

[1] P. Kuchment and L. Kunyansky, Eur. J. Appl. Math. **19**, 191 (2008).
[2] L. Wang, *Photoacoustic Imaging and Spectroscopy*, Optical Science and Engineering (CRC, Boca Raton, FL, 2009).
[3] D. Colton and R. Kress, *Inverse Acoustic and Electromagnetic Scattering Theory*, 3rd ed. (Springer, 2013).
[4] V. E. Gusev and A. A. Karabutov, *Laser Optoacoustics* (American Institute of Physics, New York, 1993).
[5] L. D. Landau and E. M. Lifshitz, *Fluid Mechanics*, 2nd ed. (Pergamon, 1987).
[6] I. Stoffels, S. Morscher, I. Helfrich, U. Hillen, J. Leyh, N. C. Burton, T. C. P. Sardella, J. Claussen, T. D. Poeppel, H. S. Bachmann, A. Roesch, K. Griewank, D. Schadendorf, M. Gunzer, and J. Klode, Sci. Transl. Med. **7**, 317ra199 (2015).
[7] I. Stoffels, S. Morscher, I. Helfrich, U. Hillen, J. Leyh, N. C. Burton, T. C. P. Sardella, J. Claussen, T. D. Poeppel, H. S. Bachmann, A. Roesch, K. Griewank, D. Schadendorf, M. Gunzer, and J. Klode, Sci. Transl. Med. **7**, 319er8 (2015).
[8] M. Xu and L. V. Wang, Phys. Rev. E **71**, 016706 (2005).
[9] K. P. Köstli, D. Frauchiger, J. J. Niederhauser, G. Paltauf, H. P. Weber, and M. Frenz, IEEE J. Sel. Top. Quantum Electron. **7**, 918 (2001).
[10] Y. Xu and L. V. Wang, Phys. Rev. Lett. **92**, 033902 (2004).
[11] P. Burgholzer, G. J. Matt, M. Haltmeier, and G. Paltauf, Phys. Rev. E **75**, 046706 (2007).
[12] G. Paltauf, J. A. Viator, S. A. Prahl, and S. L. Jacques, J. Acoust. Soc. Am. **112**, 1536 (2002).
[13] A. Karabutov, N. B. Podymova, and V. S. Letokhov, Appl. Phys. B **63**, 545 (1996).
[14] A. C. Tam, Rev. Mod. Phys. **58**, 381 (1986).
[15] R. A. Kruger, P. Liu, Y. Fang, and C. R. Appledorn, Med. Phys. **22**, 1605 (1995).

[16] Note that Ref. [15] put the heat conduction equation under scrutiny, finding that for pulse durations $t_p < 1\mu$s and absorption lengths $\ell > 1$mm, the rate of temperature change exceeds thermal diffusion in tissue by a factor of already $\approx 10^6$. Here, we might consider absorption lengths of $\ell \approx 1$mm and pulse durations $t_p \approx 10$ ns, thus justifying the thermal confinement approximation in our hypothetical case.

[17] Note that formally, the temporal δ function might be represented by a sequence of functions $\delta_{t_p}(t) = (\pi t_p)^{-1/2} \exp -(t/t_p)^2$ in the limit $\delta(t) = \lim_{t_p \to 0} \delta_{t_p}(t)$. If we assume a hypothetical situation with absorption lengths of $\ell \approx 1$ mm and sound velocity $c = 1500$ m/s, this yields typical propagation times of $\approx 1\ \mu$s. Thus, pulse durations of $t_p \approx 10$ ns might suffice to approve stress confinement.

[18] G. Paltauf and H. Schmidt-Kloiber, J. Appl. Phys. **88**, 1624 (2000).

[19] Note that, so as to exclude the nonphysical effect of a point source on itself, the Poisson integral has to be understood in terms of its principal value if the source volume V' contains the field point $\vec{r}$.

[20] G. Paltauf and H. Schmidt-Kloiber, J. Appl. Phys. **82**, 1525 (1997).

[21] G. Paltauf, H. Schmidt-Kloiber, and M. Frenz, J. Acoust. Soc. Am. **104**, 890 (1998).

[22] M. A. Afromowitz, P. S. Yeh, and S. Yee, J. Appl. Phys. **48**, 209 (1977).

[23] M. Jaeger, J. J. Niederhauser, M. Hejazi, and M. Frenz, J Biomed. Opt. **10**, 024035 (2005).

[24] E. Blumenröther, O. Melchert, M. Wollweber, and B. Roth, Photoacoustics **4**, 125 (2016).

[25] O. Melchert, SONOS—A fast Poisson integral solver for layered homogeneous media, https://github.com/omelchert/SONOS.git (2016).

[26] W. Press, B. Flannery, S. Teukolsky, and W. Vetterling, *Numerical Recipes in FORTRAN 77*, Numerical Recipes in FORTRAN: The Art of Scientific Computing (Cambridge University Press, Cambridge, 1992).

[27] M. Hazewinkel, *Encyclopaedia of Mathematics*, Encyclopaedia of Mathematics: An Updated and Annotated Translation of the Soviet "Mathematical Encyclopaedia" (Springer, 1987).

[28] D. Michie, Nature (London) **218**, 19 (1968).

[29] M. W. Sigrist, J. Appl. Phys. **60**, R83 (1986).

[30] C. Terzić and M. W. Sigrist, J. Appl. Phys. **56**, 93 (1984).

[31] K. Mitsuhashi, K. Wang, and M. A. Anastasio, Photoacoustics **2**, 21 (2014).

[32] E. Hairer, S. P. Nørsett, and G. Wanner, *Solving Ordinary Differential Equations I: Nonstiff Problems*, 2nd revised ed. (Springer-Verlag, New York, 1993).

[33] Note that such an approach might be considered as committing inverse crime [34], i.e., performing a (putative) trivial inversion of synthetic data obtained by first solving the forward problem in terms of the same exact model. However, here we use this approach as a proof of principle and consider an independent forward solver (with no connection to the Volterra-based solver) in subsequent sections.

[34] D. Colton and R. Kress, *Inverse Acoustic and Electromagnetic Scattering Theory* (Springer Science & Business Media, 2012), Vol. 93.

[35] M. Rahlves, A. Varkentin, J. Stritzel, E. Blumenröther, M. Mazurenka, M. Wollweber, and B. Roth, Proc. SPIE **9701**, 97010F (2016).